Effect of alloy composition on catalytic performance and coke-resistance property of Ni-Cu/Mg(Al)O catalysts for dry reforming of methane

Kai Song[a], Miaomiao Lu[a], Shuping Xu[a], Chongqi Chen[a], Yingying Zhan[a], Dalin Li[a,*],
Chaktong Au[a], Lilong Jiang[a], Keiichi Tomishige[b]

[a] National Engineering Research Center of Chemical Fertilizer Catalyst (NERC-CFC), College of Chemical Engineering, Fuzhou University, Gongye Road No. 523, Fuzhou 350002, Fujian, PR China
[b] Department of Applied Chemistry, School of Engineering, Tohoku University, 6-6-07, Aoba, Aramaki, Aoba-ku, Sendai 980-8579, Japan

ARTICLE INFO

ABSTRACT

In $CH_4 - CO_2$ reforming, the activity and coke resistance of hydrotalcite-derived Ni-Cu/Mg(Al)O alloy catalysts show strong dependence on Ni-Cu composition. At reaction conditions of $T = 873$ K, $CH_4/CO_2/N_2 = 1/1/2$, $SV = 60\ 000$ mL h^{-1} g^{-1}, and TOS = 25 h, the alloy catalysts with bulk Cu/Ni ratio of 0.25–0.5 exhibit good activity, stability, and coke resistance, while those with lower and higher Cu/Ni ratios deactivate due to severe coking. The optimized Ni-Cu/Mg(Al)O catalysts show graphitic carbon which is only 1/85–1/136 that of Ni/Mg (Al)O, highlighting the efficacy of Ni-Cu alloying for coke suppression. Moreover, the Ni-Cu/Mg(Al)O catalyst of highest activity performs well at temperature as low as 723 K, appearing as an effective non-precious catalysts for low-temperature $CH_4 - CO_2$ reforming. It is disclosed that a Cu composition of 25–45% is appropriate for the alloy catalyst to perform well. The results of activation energy measurement, CH_4-TPSR/O_2-TPO, and CO_2-TPSR/ H_2-TPR indicate that alloying Ni with Cu inhibits CH_4 decomposition, and Cu provides sites for CO_2 dissociation to yield more active oxygen species suitable for carbon gasification, consequently lowering coke deposition and enhancing catalytic stability.

1. Introduction

From the viewpoints of environment protection and sustainable energy, dry reforming of methane (DRM) with carbon dioxide to synthesis gas (syngas) is attractive. CH_4 and CO_2 are major greenhouse gases that exist in abundance, while syngas is the building block for a wide variety of fuels and chemicals such as methanol, Fischer-Tropsch oils, and dimethyl ether. One advantage of DRM is the direct use of CH_4 and/or CO_2 without the need of having them separated in cases such as flue gas, biogas, and non-conventional natural gas. For DRM, catalysts that are based on group VIII metals such as Pt, Rh, Ru, Ni, and Co are catalytically active. Among them, the Ni-based ones are the most widely investigated because of their low cost and relatively high activity. However, they are prone to coke deposition, metal oxidation, and sintering of metal particles. Coke deposition originates mainly from methane decomposition and/or Boudouard reactions. Deactivation due to coking is recognized as the biggest challenge for Ni catalysts, and great efforts have been made to develop active, stable, and coke-resistant Ni catalysts for $CH_4 - CO_2$ reforming [1–20].

One effective way to improve the catalytic performance of Ni catalysts is to have Ni alloyed with another metal such as Fe, Co, or Cu. There are investigations on the effect of Ni-Cu alloying on $CH_4 - CO_2$ reforming [21–30]. Two decades ago, Halliche et al. [21] reported that the addition of Cu to Ni/α-Al$_2$O$_3$ would lead to decrease of activity and increase of coke deposition. Recently, Wu et al. [22] reported decreased activity over encapsulated Ni-Cu@SiO$_2$ catalysts, but increased activity over a Ni-Cu/SiO$_2$ hierarchical catalyst [23]. Zhang et al. [24] reported a Ni-Cu-Mg-Al bimetallic catalyst that showed relatively low activity at 1023 K as compared to the Ni-Co, Ni-Fe, and Ni-Mn catalysts. Catalyst deactivation was also observed by Rahemi et al [25] on a 10%Ni-3%Cu/γ-Al$_2$O$_3$ catalyst, whereas Yu et al. [26] reported a significant improvement of catalytic stability and coke resistance on Ni$_{0.15}$Cu$_{0.05}$Mg$_{1.8}$AlO$_{3.5}$, but the activity was slightly lower as compared to Ni$_{0.2}$Mg$_{1.8}$AlO$_{3.5}$. Lee et al. [27] reported that the addition of 1% Cu to 10%Ni/γ-Al$_2$O$_3$ catalyst enhanced catalytic activity and stability at 1023 K, while addition of over 5% Cu accelerated catalyst deactivation and coke deposition. Similarly, Chen et al. [28] reported that an 8%Ni-1%Cu/SiO$_2$ catalyst showed enhanced activity and stability at 1073 K, but catalytic stability decreased when the copper content exceeded 2.0% and when the reaction temperature was below 1033 K. Indeed,

---

works on this area in the past 20 years are inconclusive. Overall, despite most of the Ni-Cu catalysts showed better reforming stability and lower coke deposition, activity loss is a major concern. It is apparent that catalytic activity, stability, and coke deposition behavior of a Ni-Cu alloy catalyst are influenced by parameters such as reaction temperature, catalyst composition and structure, support morphology, and preparation method. It should be mentioned that most of the above studies were conducted at high temperatures (> 973 K), while very few at low temperatures (e.g. ≤ 873 K). Since coke deposition becomes more prominent at reduced temperatures, catalytic studies of Ni-Cu alloy catalysts at low temperatures are necessary to better understand the effect of Ni-Cu alloying on coke deposition. By the way, there is an interest in low-temperature DRM, which can be operated in a membrane reactor [31,32] or driven by solar energy and used as a chemical energy transmission system (CETS) [33]. Thus, development of coke-resistant catalysts for low-temperature DRM is also desired. It should be noted as well that most of the Ni-Cu alloy catalysts were prepared by conventional impregnation method [21,25,27,28,30]. This approach usually results in large-size metal particles and inhomogeneous composition, inevitably leading to the formation of Ni-rich and/or Cu-rich alloy particles [27]. This not only affects the catalytic activity but also makes it difficult to understand the effect of Ni-Cu alloying on performance.

Recently, we showed that it is possible to prepare composition-uniform alloy nanoparticles using hydrotalcite-like compounds (HTlcs) or layered double hydroxides (LDHs) as precursor [34–37]. HTlcs belong to a class of two dimensional anionic clays that consist of positively charged brucite-like layers and exchangeable interlayer anions expressed as $[M_{1-x}^{2+}M_x^{3+}(OH)_2]^{x+}(A^{n-})_{x/n} \cdot mH_2O$ [38]. With metal cations M^{2+}/M^{3+} uniformly distributed in the brucite-like layers, calcination of HTlcs usually produces homogeneous mixed metal oxides and upon reduction well-dispersed metal nanoparticles. By using Ni-Fe-Mg-Al HTlcs and Ni-Cu-Mg-Al HTlcs as precursors, we prepared composition-uniform Ni-Fe and Ni-Cu catalysts that are highly active for steam reforming of biomass tar and its model compounds [34–37].

In the present work, we investigate the catalytic performance and coke deposition behavior of Ni-Cu/Mg(Al)O alloy catalysts in $CH_4 - CO_2$ reforming. Special attention was paid to the effect of alloy composition on low-temperature performance and coke resistance. The reaction was carried out at 723–873 K, significantly lower than those reported in most of the previous studies. The catalysts were characterized by techniques such as XRD, STEM-EDX, SEM, O_2-TPO, XPS, CH_4-TPSR/O_2-TPO, and CO_2-TPSR/H_2-TPR. It is found that the catalytic activity, stability, and coke resistance property of the Ni-Cu/Mg(Al)O catalysts are strongly dependent on the alloy composition. Herein, we report for the first time that the Ni-Cu/Mg(Al)O catalyst with optimized Cu/Ni ratio is highly active, stable, and coke-resistant even at temperature as low as 723 K, undeniably an outstanding catalyst for $CH_4 - CO_2$ reforming, especially at low temperatures.

2. Experimental

2.1. Catalyst preparation

Ni-Cu-Mg-Al HTlcs were prepared by co-precipitation as reported previously [37]. In brief, an aqueous solution of $Ni(NO_3)_2 \cdot 6H_2O$, $Cu(NO_3)_2 \cdot 3H_2O$, $Mg(NO_3)_2 \cdot 6H_2O$, and $Al(NO_3)_3 \cdot 9H_2O$ was added slowly into an aqueous solution of Na_2CO_3 under stirring at room temperature and a constant pH of 10 ± 0.5. The precipitate was filtered out, washed with de-ionized water, and dried at 373 K overnight, followed by calcination in air at 1073 K for 5 h. The Ni-Cu alloy catalysts were obtained by H_2 reduction of the calcined samples at 1073 K for 0.5 h. The nominal catalyst composition was Ni loading = 12 wt%, molar ratio of (Ni + Cu + Mg)/Al = 3, and molar ratio of Cu/Ni = 0.1, 0.25, 0.5, and 1.0, which were confirmed by ICP analysis (Table S1 Supplementary material). After reduction, the actual alloy composition ($Cu°/Ni°$) was

determined by XRD using Vegard's law to be 0.13, 0.33, 0.79, and 1.98, some of which were further corroborated by STEM-EDX measurements [37]. All of the calcined and reduced samples show relatively high BET surface areas of $82–156 \, m^2 \, g^{-1}$ (Table S2 Supplementary material), attributable to the formation of thermally stable Mg(Al)O mixed oxide.
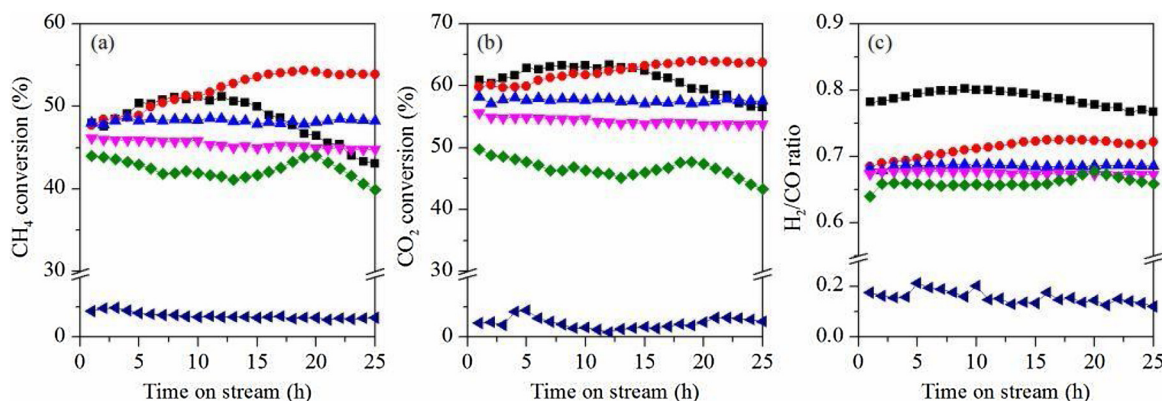
2.2. Catalytic reaction

Dry reforming of methane was performed in a fixed-bed quartz-tube reactor (i.d. 6 mm) at atmospheric pressure. For tests of catalytic activity and stability, the reaction was carried out at 723–873 K for 25 h over 50 mg of catalyst. Before the test, the catalyst was reduced with H_2 (30 mL min^{-1}) at 1073 K for 0.5 h. Subsequently, the catalyst was cooled to a designated temperature in N_2 stream before the introduction of feed gas to start the reaction. The composition of feed gas was $CH_4/CO_2/N_2 = 1/1/2$ and the total flow rate was 50 mL min^{-1}, corresponding to a space velocity of 60 000 mL h^{-1} g^{-1}. The effluent gas was online analyzed by a TCD gas chromatography (GC-2014, Shimadzu). For activation energy measurements, the reaction was conducted at $CH_4/CO_2/N_2 = 1/1/2$ and SV = 120 000 mL h^{-1} g^{-1}, and the reaction temperature was raised from 753 K to 793 K at intervals of 10 K. For each measurement, the activity was evaluated for 15 min. Under the adopted conditions, CH_4 conversion was below the equilibrium level.

2.3. Catalyst characterization

X-ray diffraction (XRD) analysis was conducted on a PANalytical X'pert Pro diffractometer equipped with Co Ka ($\lambda = 0.1789$ nm) radiation operating at 40 kV and 40 mA. Scanning transmission electronic microscopy and energy dispersive X-ray (STEM-EDX) analyses were carried out on a JEM-2100 F (JEOL) microscope operated at 200 kV. Scanning electronic microscopy (SEM) analysis was performed on a Hitachi-S4800 microscope operated at 5.0 kV.

X-ray photoelectron spectroscopy (XPS) was conducted on a Thermo Scifentific Escalab 250Xi spectrometer. The reduced sample was in situ treated with H_2 at 723 K. Spectra were taken under ultra-high vacuum condition ($< 1 \times 10^{-7}$ torr) by using Al K$_a$ radiation (1486.6 eV) generated at 300 W. Ni 2p, Cu 2p, and C1s spectra were recorded at a pass energy of 20 eV. All Ni and Cu binding energies were calibrated with respect to C1s (284.8 eV). Peak deconvolution was performed with XPS peak 41 processing software.

Temperature-programmed oxidation (O_2-TPO) and temperature-programmed surface reaction (TPSR) measurements were performed on a Micrometric AutoChem 2920, which was connected to a mass spectrometer (Hiden Analytical HPR20). O_2-TPO was used to measure coke deposition on the used catalysts. About 30 mg of used catalyst was employed. The O_2-TPO profile was recorded with the catalyst heated (10 K min^{-1}) from ambient temperature to 1073 K in a flow of 3%O_2/Ar flow (30 mL min^{-1}). The profile of CO_2 formation was integrated and used to calculate the amount of coke deposition. For CH_4-TPSR/O_2-TPO, 50 mg of catalyst was loaded and reduced with H_2 at 1073 K for 0.5 h, and then purged with Ar during cooling to room temperature. The CH_4-TPSR profile was recorded with the catalyst heated (10 K min^{-1}) from ambient temperature to 1073 K in a flow of 5%CH_4/N_2 (50 mL min^{-1}). CH_4 consumption and H_2 formation were monitored at mass signals of $m/e = 16$ and 2, respectively. Subsequent to cooling to room temperature, O_2-TPO was performed to characterize the carbon formed during CH_4-TPSR. For CO_2-TPSR/H_2-TPR, 50 mg of catalyst was reduced with H_2 at 1073 K for 0.5 h, and then purged with Ar to room temperature. Subsequently, a flow of 5%CO_2/N_2 mixed gas (50 mL min^{-1}) was introduced into the reactor and then the temperature was raised to 873 K (10 K min^{-1}) and kept at 873 K for 0.5 h. Then the system was subject to Ar purging and cooling to room temperature, and H_2-TPR was carried out to identify the oxygen species formed during CO_2-TPSR.

Fig. 1. Effect of alloy composition on catalytic performance of Ni-Cu/Mg(Al)O catalysts: (a) CH_4 conversion, (b) CO_2 conversion, and (c) H_2/CO ratio; (■) Ni, (●) Cu/Ni = 0.1, (▲) Cu/Ni = 0.25, (▼) Cu/Ni = 0.5, (♦) Cu/Ni = 1.0, and (◀) Cu. Reaction conditions: T = 873 K, $CH_4/CO_2/N_2$ = 1/1/2, SV = 60 000 mL h^{-1} g^{-1}, catalyst 50 mg, pre-reduced with H_2 at 1073 K for 0.5 h.

3. Results and discussion

3.1. Effect of alloy composition on catalytic performance

The effects of Cu/Ni ratio on the catalytic activity and stability of Ni-Cu/Mg(Al)O catalysts in $CH_4 - CO_2$ reforming were investigated at 873 K for 25 h with $CH_4/CO_2/N_2$ = 1/1/2 and SV = 60 000 mL h^{-1} g^{-1}. The changes of CH_4 conversion, CO_2 conversion, and H_2/CO ratio with time on stream over Ni-Cu/Mg(Al)O catalysts are shown in Fig. 1. The yields of H_2 and CO are presented in Fig. S1 (Supplementary material). For Ni/Mg(Al)O, CH_4 and CO_2 conversions and H_2/CO ratio first increase and then decrease with time on stream. The maximum CH_4 and CO_2 conversions and H_2/CO ratio are about 51%, 63%, and 0.8, respectively, slightly higher than those of equilibrium level which are 47.9%, 60.7%, and 0.79 according to calculation based on $CH_4 - CO_2$ reforming and reverse water-gas shift reactions. The increase of CH_4 conversion and H_2/CO ratio can be attributed to the occurrence of CH_4 decomposition [39], which is a side reaction also observed over Ce-, Zr- and La-modified Ni/Mg(Al)O catalysts [40–42], while the increase of CO_2 conversion may be interpreted as due to the enhanced reverse water-gas shift reaction by the H_2 produced from CH_4 decomposition. On the other hand, the decrease of CH_4 and CO_2 conversions and H_2/CO ratio with time on stream can be related to catalyst deactivation by coke deposition as a result of CH_4 decomposition [39]. In comparison with Ni/Mg(Al)O, the Cu counterpart shows much lower CH_4 conversion (< 5%), indicating that Cu metal is less active for the reaction. In the case of Ni-Cu/Mg(Al)O catalysts, the catalytic performance is found to be strongly dependent on alloy composition. At low Cu content (e.g. Cu/Ni = 0.1), the CH_4 and CO_2 conversions and H_2/CO ratio increase with time on stream, indicating the occurrence of CH_4 decomposition. It is noted that the CH_4 conversion at the end of test is much higher than that of Ni/Mg(Al)O. Meanwhile, the amount of coke deposition on this catalyst is larger than that on Ni/Mg(Al)O (*vide infra*). It seems that alloying Ni with a small amount of Cu facilitates CH_4 decomposition. Nonetheless, the H_2/CO ratio is lower than that of Ni/Mg(Al)O, which is probably due to the enhanced reverse water-gas shift reaction by the presence of Cu [43]. In contrast, there is drastic improvement of catalytic performance at Cu/Ni = 0.25 and 0.5; both catalysts exhibit stable activity during the whole period of investigation. The activity of Ni-Cu/Mg(Al)O (Cu/Ni = 0.25) is close to that of thermodynamic equilibrium, and slightly higher than that of Ni-Cu/Mg(Al)O (Cu/Ni = 0.5), which can be attributed to the larger amount of surface Ni° active sites as determined by H_2 chemisorption [37]. At higher Cu content (Cu/Ni = 1.0), there is decrease of activity and stability, a phenomenon similar to those observed over Ni-Cu/Al$_2$O$_3$ and Ni-Cu/SiO$_2$ catalysts [27,28]. The results indicate that there exists an optimal Ni-Cu composition for high activity and stability. According to the XRD

characterization result [37], the actual Cu°/Ni° composition is 0.33 for Cu/Ni = 0.25 and 0.79 for Cu/Ni = 0.5. Therefore, to optimize catalytic performance, an alloy composition of Cu°/Ni° = 0.33–0.79 (i.e. ~25%–45%Cu) is the most suitable for the Ni-Cu/Mg(Al)O catalysts.

To further verify the effectiveness of Ni-Cu alloying, the catalytic performance of the Ni-Cu/Mg(Al)O (Cu/Ni = 0.25) catalyst optimized in Cu/Ni ratio was investigated at lower temperatures and compared to that of Ni/Mg(Al)O. The temperature dependence of catalytic performance with time on stream at 723–873 K is shown in Fig. 2. For the Ni catalyst, CH_4 decomposition becomes more pronounced when reaction temperature is decreased from 873 K to 723 K. For example, at 823 K, the CH_4 conversion and H_2/CO ratio increase quickly within 5 h, reaching maximum values much higher than those at the equilibrium. Similar trends are also observed at 773 K and 723 K. In contrast, the Ni-Cu/Mg(Al)O catalyst exhibits stable activity at all temperatures, with CH_4 and CO_2 conversions and H_2/CO ratio close to those of equilibrium levels. Apparently, the optimized alloy catalyst is highly active and stable at 723–873 K, demonstrating its effectiveness for low-temperature $CH_4 - CO_2$ reforming.

3.2. Effect of alloy composition on coke deposition

To understand the performance discrepancy of the Ni-Cu/Mg(Al)O catalysts in $CH_4 - CO_2$ reforming, the used catalysts were characterized by XRD, STEM-EDX, SEM, and O_2-TPO measurements. Fig. 3 shows the XRD patterns of the used catalysts after reaction at 873 K for 25 h. Similar to the case of H_2-reduced catalysts ([37] or Fig. S2 Supplementary material), the diffraction peaks of Ni metal become weakened, broadened and shifted to lower angles as a result of Ni-Cu alloying. The formation of Ni-Cu alloy is also confirmed by STEM-EDX analysis (Fig. 4). Taking Ni-Cu/Mg(Al)O (Cu/Ni = 0.25) as an example, the HAADF-STEM images and EDX analysis clearly reveal the presence of Ni and Cu within a single particle. The alloy composition determined by EDX is Cu°/Ni° = 0.30 and the average particle size calculated by $\Sigma n_i d_i^3 / \Sigma n_i d_i^2$ is 7.4 nm. Both values are similar to those of the H_2-reduced counterpart [37], suggesting that Ni-Cu alloy nanoparticles are stable during the reaction.

In the XRD patterns of used Ni/Mg(Al)O, Ni-Cu/Mg(Al)O (Cu/Ni = 0.1, 1.0), and Cu/Mg(Al)O catalysts, there is the detection of a peak assignable to graphitic carbon, which is not observed over the H_2-reduced counterparts ([37] or Fig. S2), indicative of severe coke deposition on the used catalysts. The SEM images (Fig. 5a, b, e, and f) also reveal the presence of a large number of carbon filaments. In contrast, over used Ni-Cu/Mg(Al)O (Cu/Ni = 0.25–0.5), there is no detection of the graphitic peak and no sight of carbon filaments (Fig. 5c and d), indicating that coke deposition is minimal.

To quantify coke deposition, O_2-TPO was carried out over the used
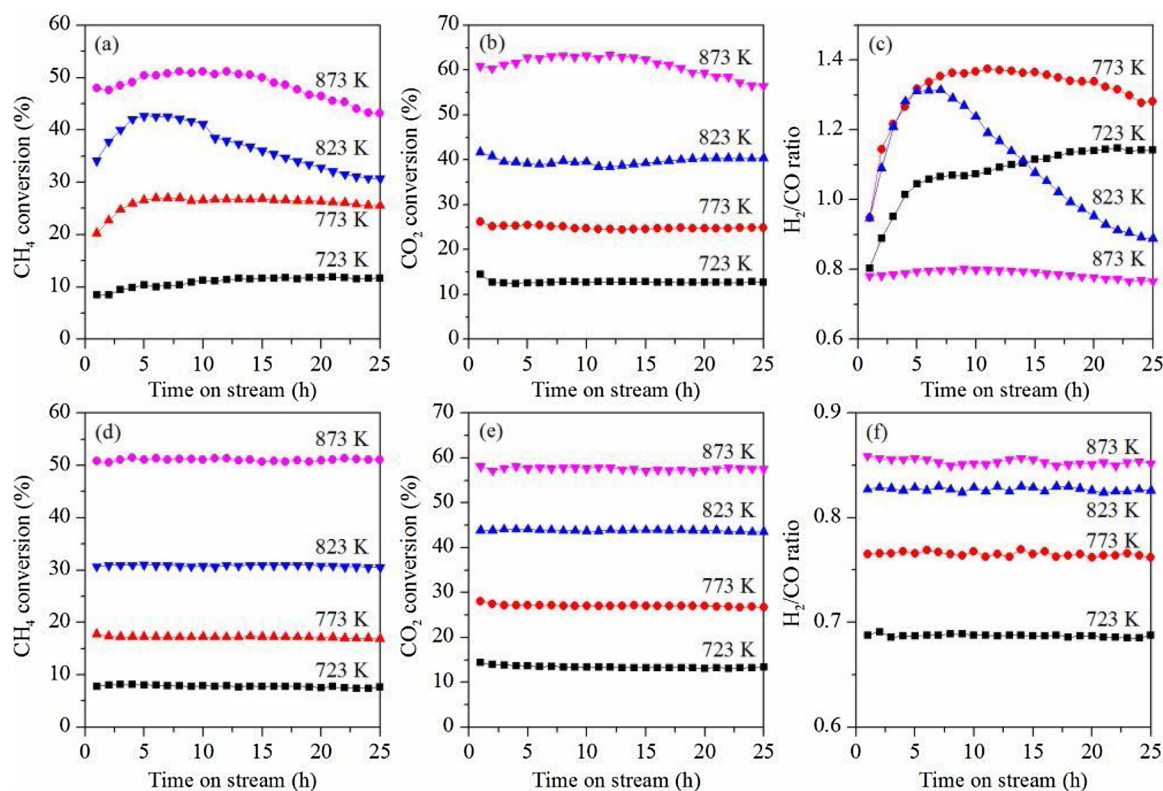
Fig. 2. Temperature dependence of catalytic performance with time on stream over (a–c) Ni/Mg(Al)O and (d–f) Ni-Cu/Mg(Al)O (Cu/Ni = 0.25) catalysts. Reaction conditions: T = 723–873 K, $CH_4/CO_2/N_2$ = 1/1/2, SV = 60 000 mL h^{-1} g^{-1}; catalyst 50 mg, pre-reduced with H_2 at 1073 K for 0.5 h.
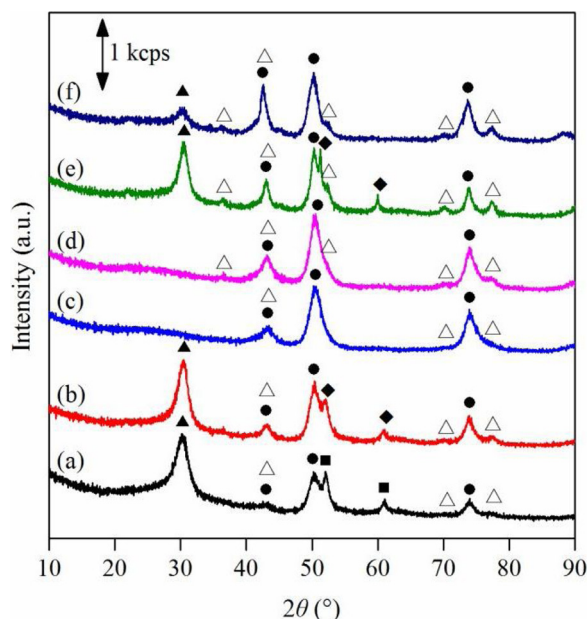
Fig. 3. XRD patterns of used catalysts: (a) Ni, (b) Cu/Ni = 0.1, (c) Cu/Ni = 0.25, (d) Cu/Ni = 0.5, (e) Cu/Ni = 1.0, and (f) Cu. Crystalline phases: (●) MgO-like phase, (■) Ni metal, (◆) Ni-Cu alloy, (△) MgAl$_2$O$_4$ spinel, and (▲) graphite. Reaction conditions: T = 873 K, $CH_4/CO_2/N_2$ = 1/1/2, SV = 60 000 mL h^{-1} g^{-1}, TOS = 25 h.

catalysts (Fig. 6). The amounts of coke deposition and average coking rates are listed in Table 1. In agreement with the XRD and SEM results, coke deposition changes remarkably with alloy composition. For Ni-Cu/Mg(Al)O (Cu/Ni = 0.25–0.5), there are only two small CO_2 peaks at 560 K and 900 K, while the other catalysts show one broad and strong

CO_2 peak at temperatures ranging from 673 K to 1073 K. The low-temperature CO_2 peak (< 673 K) can be attributed to the oxidation of active carbon intermediate, while the high-temperature one (> 673 K) to the oxidation of graphitic carbon (e.g. encapsulating carbon, filamentous carbon) [19,20,44]. As shown in Table 1, at Cu/Ni = 0.1, coke deposition is slightly larger than that of Ni/Mg(Al)O, indicating that Ni-Cu alloy with low Cu content promotes coke formation. Interestingly, at Cu/Ni = 0.25 and 0.5, coke deposition is significantly inhibited. The total amount of coke is only 1/55 and 1/95 that of Ni/Mg(Al)O, whereas for graphitic carbon, it is about 1/85 and 1/136 that of Ni/Mg(Al)O, respectively. The results indicate the positive effect of Ni-Cu alloying on the suppression of coke deposition. As expected, coke deposition increases again at Cu/Ni = 1.0. It is thus evidenced that alloying Ni with 25%–45% Cu is effective for the suppression of coke deposition, while a Cu content lower 25% or higher than 45% worsens coke deposition.

Compared in Table 2 are the coke depositions over Ni/Mg(Al)O and Ni-Cu/Mg(Al)O (Cu/Ni = 0.25) at different reaction temperatures. The XRD patterns and O_2-TPO files of the used catalysts are provided in Figs. S3 and S4 (Supplementary material). For the Ni catalyst, coke deposition does not change markedly with decreasing reaction temperature from 873 K to 723 K. Nonetheless, when normalized to CH_4 conversion (Table S3 Supplementary material), coke deposition per CH_4 conversion increases with the decrease of reaction temperature, indicating that coke is more easily formed at low temperatures. For the Ni-Cu catalyst, coke deposition is effectively suppressed with the decrease of reaction temperature. At 823 K, graphitic carbon on the Ni-Cu catalyst is similar to that at 873 K, which is about 1/87 that on the Ni catalyst. This value decreases to ∼1/320 at 773 K and even to ∼1/1800 at 723 K, demonstrating the excellent coke resistance of Ni-Cu/Mg(Al)O (Cu/Ni = 0.25) catalyst at low temperatures.

To illustrate the effectiveness of the optimized Ni-Cu/Mg(Al)O (Cu/Ni = 0.25) catalyst for DRM, a comparison with several representative Ni-Cu alloy catalysts is made in terms of catalytic activity, stability, and
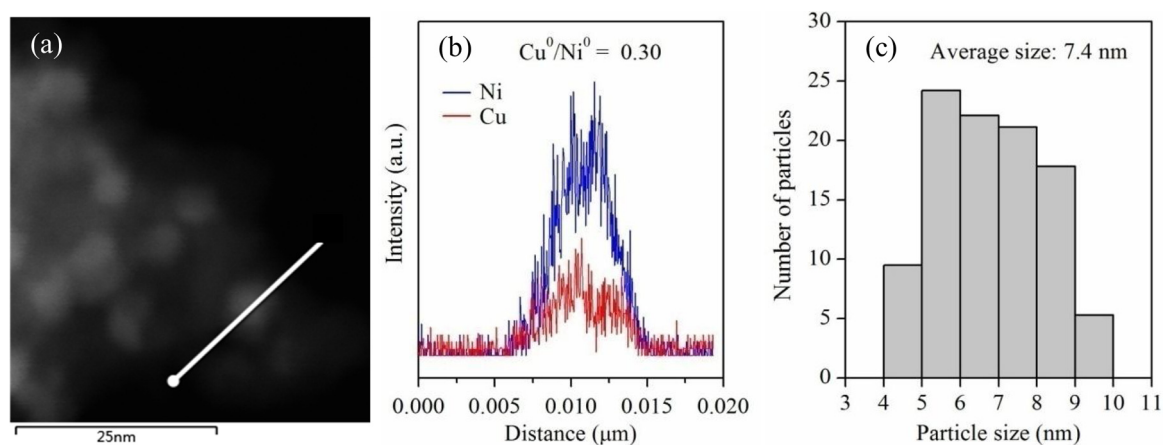
Fig. 4. (a) HAADF-STEM image, (b) EDX elementary analysis, and (c) particle size distribution of Ni-Cu/Mg(Al)O (Cu/Ni = 0.25) used catalyst.
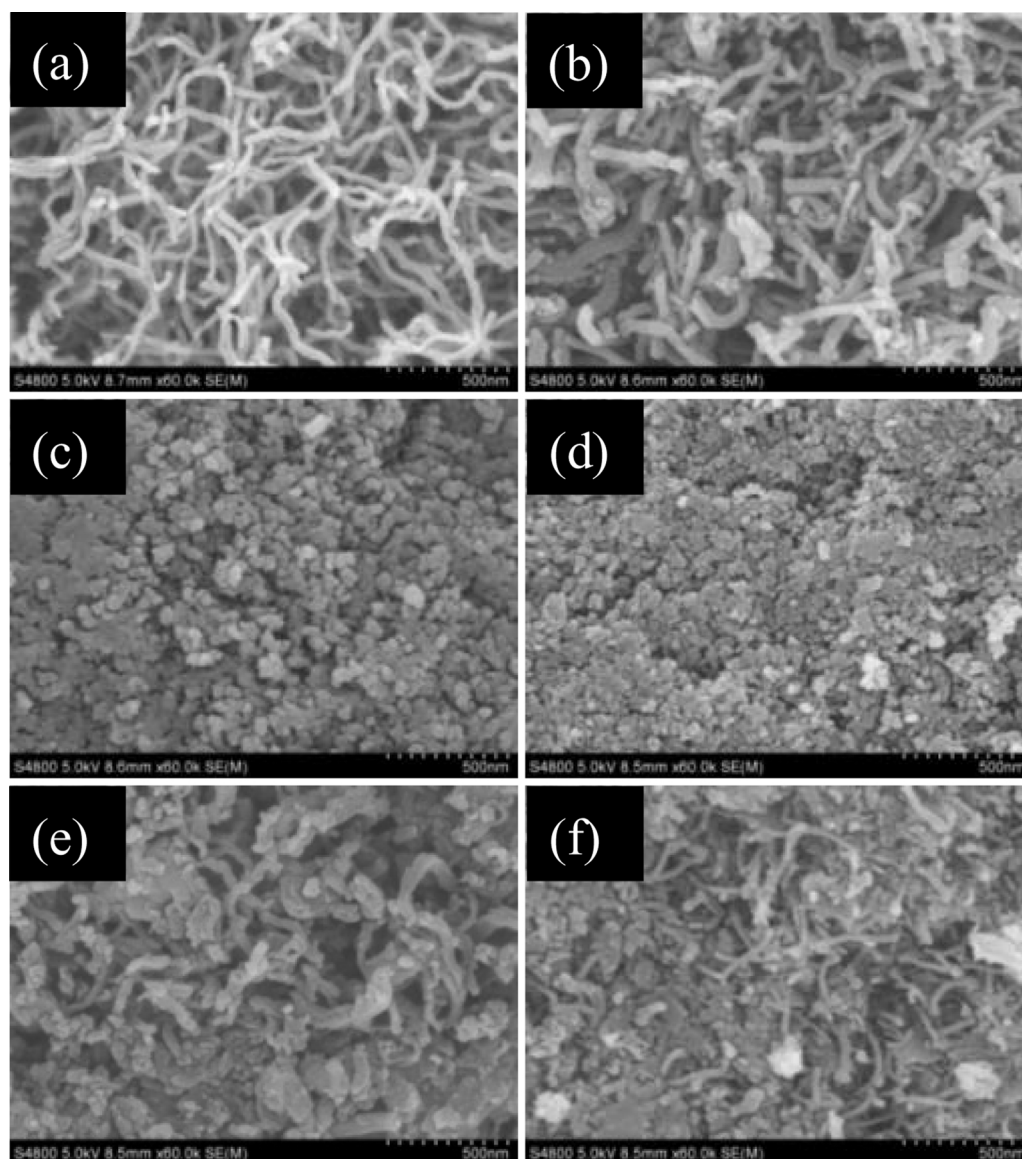

Fig. 5. SEM images of used catalysts: (a) Ni, (b) Cu/Ni = 0.1, (c) Cu/Ni = 0.25, (d) Cu/Ni = 0.5, (e) Cu/Ni = 1.0, and (f) Cu. Reaction conditions: T = 873 K, CH_4/CO_2/N_2 = 1/1/2, SV = 60 000 mL h^{-1} g^{-1}, TOS = 25 h.
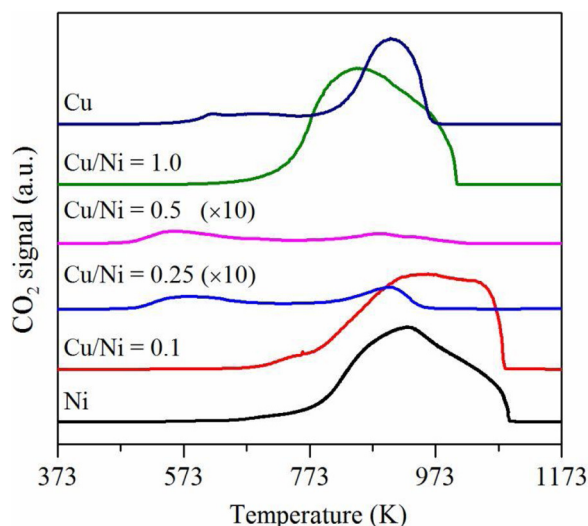
Fig. 6. O$_2$-TPO profiles of coke deposition on used catalysts. Reaction conditions: T = 873 K, CH$_4$/CO$_2$/N$_2$ = 1/1/2, SV = 60 000 mL h^{-1} g^{-1}, and TOS = 25 h.

coke deposition (Table S4 Supplementary material). Generally, addition of a suitable amount of Cu to Ni catalyst leads to better activity, while addition of an excess amount of Cu leads to poorer performance [27,28], in agreement with the results of the present study. Concerning optimized alloy composition, Lee et al. [27] reported Cu°/Ni° of 0.1–0.5 for Ni-Cu/γ-Al$_2$O$_3$ catalyst, and Chen et al. [28] reported Cu°/Ni° of 0.12–0.2 for Ni-Cu/SiO$_2$ catalyst, both of which are different with that for the optimized Ni-Cu/Mg(Al)O catalysts presented in this work. This may be attributed to the difference in particle size and composition inhomogeneity as well as discrepancy in support and reaction condition. There are several supported Ni-Cu alloy catalysts that show stable activity at temperatures below 973 K [22,23,30]. Nonetheless, only the Ni-Cu/Mg(Al)O (Cu/Ni = 0.25) of the present work exhibits high catalytic stability at temperature as low as 723 K. To the best of our knowledge, only limited number of catalysts, such as the hydrotalcite-derived Co/Mg(Al)O catalyst, were reported to show stable activity at temperatures below 773 K [39,45,46] (Table S5 Supplementary material). It is noted that Ni-Cu/Mg(Al)O (Cu/Ni = 0.25) is superior to Co/Mg(Al)O in terms of coke resistance; the latter shows an average total coking rate of 3.4 mg-C g$_{cat}^{-1}$ h^{-1}, about 4 times that of the former at 773 K. It is considered that the Ni-Cu/Mg(Al)O (Cu/Ni = 0.25) catalyst is one of the most effective non-precious catalysts for low-temperature DRM.

3.3. Role of Ni-Cu alloying in coke suppression

3.3.1. XPS

As presented above, the nature of coke deposition on Ni-Cu/Mg(Al)O catalysts varies significantly with alloy composition. The different behaviors are plausibly due to the different states of Cu in the Ni-Cu alloy particles. To investigate the surface state of Ni-Cu alloy, XPS was carried out. Fig. 7 shows the Ni 2p and Cu 2p XPS of the reduced catalysts and the result of peak deconvolution is summarized in Table 3. For Ni/Mg(Al)O, the peaks at 856.1 and 874.4 eV as well as the satellite peaks at 861.8 and 879.6 eV can be assigned to Ni^{2+} 2p$_{3/2}$ and 2p$_{1/2}$, whereas those at 852.9 and 870.8 eV can be attributed to Ni° 2p$_{3/2}$ and 2p$_{1/2}$, respectively [19,47]. The presence of Ni^{2+} is a result of strong interaction between NiO and Mg(Al)O that requires temperature higher than 1223 K for complete reduction of Ni^{2+} species [36]. For Cu/Mg(Al)O, there are two peaks at 932.8 and 953.0 eV corresponding to Cu° 2p$_{3/2}$ and 2p$_{1/2}$ [47]. No obvious peaks due to Cu^{2+} are detected, indicating that Cu species are almost completely reduced [37]. The Ni 2p and Cu 2p XPS of Ni-Cu/Mg(Al)O are similar to those of Ni/Mg(Al)O and Cu/Mg(Al)O. From Ni° 2p$_{3/2}$ and Cu° 2p$_{3/2}$ peaks, the alloy surface composition (Cu°$_s$/Ni°$_s$) is calculated. It is shown that the surface Cu°/Ni° ratios are much higher than the bulk ones [37], suggesting that Cu is enriched on the alloy surface. This is consistent with the reports [48–50] that Cu segregates on the surface of the Ni-Cu particles, driven by the lower surface energy of Cu compared with Ni [51].

According to the literature [51], surface-segregated Cu atoms preferentially occupy the flat terrace sites of Ni because of the small lattice size mismatch between Cu and Ni (a_0 (Cu) = 0.362 nm; a_0 (Ni) = 0.354 nm). Thus, a low concentration of Cu is not sufficient enough to suppress coke deposition. This is in part supported by the result reported by Alstrup et al. [52] that a small amount of Cu in Ni-Cu/SiO$_2$ (Cu/Ni = 1/99) promotes carbon formation in CH$_4$ decomposition. With the increase of Cu content, Cu atoms start to occupy most of the edge and kink Ni sites responsible for carbon formation [53], resulting in effective suppression of coke deposition. In the case when Cu is in excess, there would be the formation of Cu clusters [54]. Considering the large coke deposition on Cu/Mg(Al)O, we deduce that the Cu clusters catalyze carbon formation, acting like Cu metal in CH$_4$−CO$_2$ reforming.

3.3.2. Activation energy measurement

For CH$_4$−CO$_2$ reforming and other CH$_4$ reforming reactions, CH$_4$ dissociation is generally believed to be rate-determining. To get more information about the effect of Ni-Cu alloying on CH$_4$ dissociation, the activation energy of CH$_4$−CO$_2$ reforming was measured at conditions of T = 753–793 K, CH$_4$/CO$_2$/N$_2$ = 1/1/2, and SV = 120 000 mL h^{-1} g^{-1}. Fig. 8 shows the Arrhenius plots of CH$_4$−CO$_2$ reforming over Ni/Mg(Al)O and Ni-Cu/Mg(Al)O (Cu/Ni = 0.25). The calculated CH$_4$ activation energies are listed in Table 4 together with the activity data at 773 K. For the Ni catalyst, E_a−CH$_4$ is 51.8 kJ mol^{-1}. According to the literature [55], E_a−CH$_4$ on supported Ni catalysts varies from 33.5 to 100 kJ mol^{-1} depending on the kind of support materials, and a value of 58.6 ± 4.2 kJ mol^{-1} is the most frequently reported, which coincides those of 55.6 ± 6.3 and 52.7 ± 5.0 kJ mol^{-1} for CH$_4$ dissociation on Ni(110) and Ni(111), respectively [56]. This is in good agreement with our result. By alloying Ni with Cu, E_a−CH$_4$ is increased to 62.7 kJ mol^{-1}, suggesting that Ni-Cu alloying inhibits CH$_4$ dissociation. Based

Table 1
Effect of alloy composition on coke deposition.

Catalyst	Amount of coke (wt%)			Coking rate (mg-C g$_{cat}^{-1}$ h^{-1})		
	< 673 K	> 673 K	Total	< 673 K	> 673 K	Total
Ni/Mg(Al)O	–	66.7	66.7	–	26.7	26.7
Ni-Cu/Mg(Al)O (Cu/Ni = 0.1)	–	71.2	71.2	–	28.5	28.5
Ni-Cu/Mg(Al)O (Cu/Ni = 0.25)	0.6	0.8	1.4	0.2	0.6	0.8
Ni-Cu/Mg(Al)O (Cu/Ni = 0.5)	0.6	0.5	1.1	0.2	0.2	0.4
Ni-Cu/Mg(Al)O (Cu/Ni = 1.0)	–	72.9	72.9	–	29.0	29.0
Cu/Mg(Al)O	1.8	32.2	34.0	0.7	12.9	13.6

Reaction conditions: T = 873 K, CH$_4$/CO$_2$/N$_2$ = 1/1/2, SV = 60 000 mL h^{-1} g^{-1}, TOS = 25 h.

Table 2
Effect of reaction temperature on coke deposition.

Catalyst	Temperature (K)	Amount of coke (wt%)			Coking rate (mg-C g_{cat}^{-1} h^{-1})		
		< 673 K	> 673 K	Total	< 673 K	> 673 K	Total
Ni/Mg(Al)O	873	–	66.7	66.7	–	26.7	26.7
	823	–	50.6	50.6	–	20.2	20.2
	773	–	76.7	76.7	–	30.7	30.7
	723	–	72.2	72.2	–	28.9	28.9
Ni-Cu/Mg(Al)O (Cu/Ni = 0.25)	873	0.62	0.78	1.4	0.25	0.56	0.81
	823	0.53	0.58	1.1	0.21	0.23	0.44
	773	0.46	0.24	0.7	0.18	0.10	0.28
	723	0.36	0.04	0.4	0.14	0.02	0.16

Reaction conditions: T = 723–873 K, $CH_4/CO_2/N_2$ = 1/1/2, SV = 60 000 mL h^{-1} g^{-1}, TOS = 25 h.

on the H_2 chemisorption [37] and the CH_4 conversion at 773 K, the turnover frequency (TOF) of CH_4 was calculated. It is shown that the Ni-Cu catalyst has a lower TOF than Ni catalyst, suggesting again that Ni-Cu alloy is less active for CH_4 dissociation than Ni metal. The inhibition of CH_4 dissociation by Ni-Cu alloying may be related to the occupation of Ni edge and kink sites that are highly active for C–H dissociation by Cu atoms [53].

3.3.3. CH_4-TPSR/O_2-TPO

The effect of Ni-Cu alloying on CH_4 dissociation was further studied by CH_4-TPSR. The obtained profiles are presented in Fig. 9(a). As expected, Ni/Mg(Al)O shows good activity for CH_4 decomposition, which starts from about 623 K and peaks at 807 K together showing a small shoulder at 634 K. In comparison to Ni/Mg(Al)O, Cu/Mg(Al)O is much less active for CH_4 decomposition, which takes place only to a small extent even the temperature is extended to 1023 K. By alloying Ni with Cu, the occurrence of CH_4 decomposition shifts to higher temperatures (by ~60 K), beginning at 685 K and reaching maximum at 897 K, displaying a shoulder peak at 694 K. This is in accordance with the increased CH_4 activation energy for CH_4 dissociation in $CH_4 - CO_2$ reforming over Ni-Cu/Mg(Al)O (Cu/Ni = 0.25), confirming that alloying Ni with Cu inhibits CH_4 decomposition.

O_2-TPO was then conducted to determine the nature and reactivity of the surface carbon species resulted from CH_4 decomposition. As shown in Fig. 9(b), Ni/Mg(Al)O shows two strong CO_2 peaks at 742 K and 903 K, while Ni-Cu/Mg(Al)O (Cu/Ni = 0.25) gives two strong CO_2 peaks at 712 K and 868 K together with a shoulder peak at 626 K. As for

**Table 3**
Ni 2p and Cu 2p XPS results of the reduced catalysts.

| Catalyst	Binding energy[a] (eV)			Surface composition of alloy $(Cu°_s/Ni°_s)$[b]
	Ni° $2p_{3/2}$	Ni^{2+} $2p_{3/2}$	Cu° $2p_{3/2}$	
Ni/Mg(Al)O	852.9 (35.3)	856.1 (64.7)	–	–
Ni-Cu/Mg(Al)O (Cu/Ni = 0.1)	852.8 (32.3)	855.9 (67.7)	932.9	0.39
Ni-Cu/Mg(Al)O (Cu/Ni = 0.25)	852.9 (32.2)	856.0 (67.8)	932.8	0.80
Ni-Cu/Mg(Al)O (Cu/Ni = 0.5)	853.2 (35.9)	856.2 (64.1)	932.8	1.24
Ni-Cu/Mg(Al)O (Cu/Ni = 1.0)	853.2 (20.2)	856.1 (79.8)	932.9	3.30
Cu/Mg(Al)O	–	–	932.8	–

[a] Numbers in parentheses represents the relative contribution obtained from peak deconvolution.
[b] Calculated from the peak area ratio of $Cu°2p_{3/2}/Ni°2p_{3/2}$ × 1.14.

Cu/Mg(Al)O, there are three small CO_2 peaks at 603, 723, and 830 K attributable to active carbon intermediate, encapsulating carbon, and filamentous carbon, respectively. Considering the profiles of the corresponding monometallic catalysts, the low-temperature CO_2 peak (< 673 K) detected over the Ni-Cu catalyst may be related to carbon species on Cu, whereas the high-temperature CO_2 peaks (> 673 K) to carbon species on Ni. It can be seen that the high-temperature CO_2
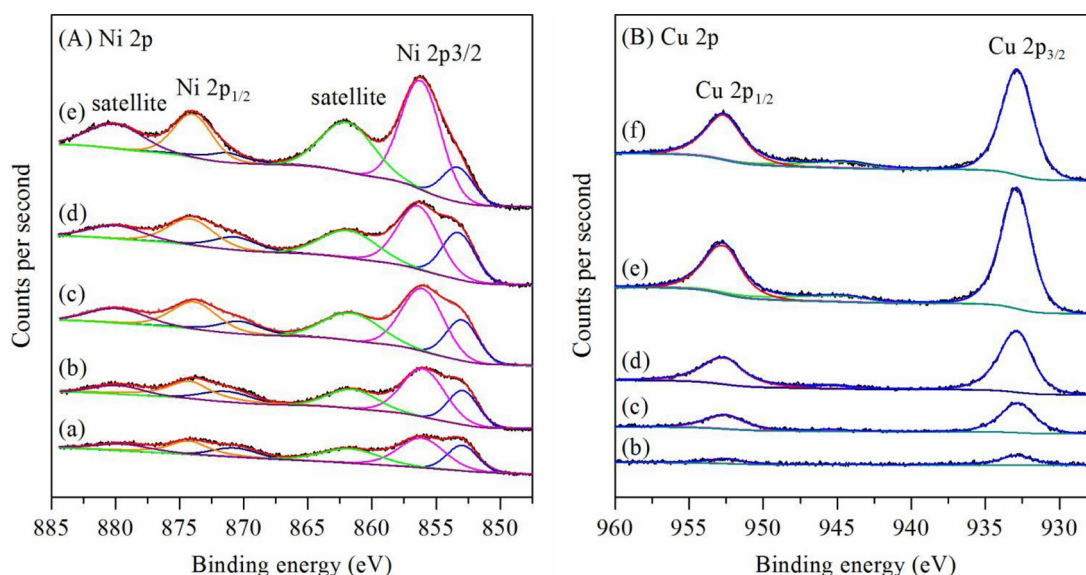
Fig. 7. (A) Ni 2p XPS and (B) Cu 2p XPS of the reduced catalysts: (a) Ni, (b) Cu/Ni = 0.1, (c) Cu/Ni = 0.25, (d) Cu/Ni = 0.5, (e) Cu/Ni = 1.0, and (f) Cu.
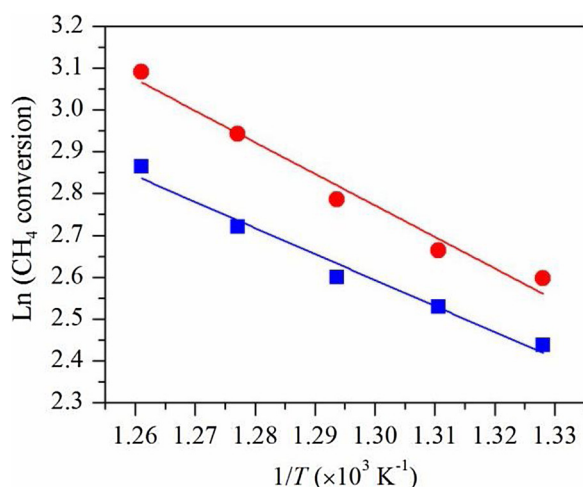
Fig. 8. Arrhenius plots of $CH_4 - CO_2$ reforming over (■) Ni/Mg(Al)O and (●) Ni-Cu/Mg(Al)O (Cu/Ni = 0.25) catalysts. Reaction conditions: T = 753–793 K, $CH_4/CO_2/N_2 = 1/1/2$, SV = 120 000 mL h^{-1} g^{-1}, catalyst 50 mg.

Table 4
Activation energy, activity, and turnover frequency.

Catalyst	CH$_4$ conversion (%)	E_a-CH$_4$ (kJ mol^{-1})	TOF-CH$_4$ (s^{-1})
Ni/Mg(Al)O	13.5	51.8	0.59
Ni-Cu/Mg(Al)O (Cu/Ni = 0.25)	16.2	62.7	0.47

Reaction conditions: T = 753–793 K, $CH_4/CO_2/N_2$ = 1/1/2, SV = 120 000 mL h^{-1} g^{-1}.

peaks detected over Ni-Cu/Mg(Al)O (Cu/Ni = 0.25) is similar to that over Ni/Mg(Al)O in shape and intensity, suggesting that the type and amount of carbon are little influenced by Ni-Cu alloying. Nonetheless, these CO_2 peaks are shifted to lower temperatures (by ~ 30 K) in the former case, implying easier oxidation and removal of deposited carbon. It is envisioned that under the reaction conditions for $CH_4 - CO_2$ reforming, the carbon species originated from CH_4 dissociation on Ni-Cu/Mg(Al)O can be gasified more readily by the oxygen species derived from CO_2 dissociation, enhancing carbon gasification and suppressing carbon deposition as a result.

3.3.4. CO$_2$-TPSR/H$_2$-TPR

CO_2 activation is also a crucial step in $CH_4 - CO_2$ reforming, which yields CO* and O*, with the latter oxidizing CH_x* to produce CO and H_2. To get information on CO_2 activation and the state of O* species, CO_2-TPSR/H$_2$-TPR was performed over the optimized Ni-Cu/Mg(Al)O catalyst. In CO_2-TPSR, CO_2 was activated at elevated temperatures (up to 873 K), and then the adsorbed O* species were characterized with H$_2$-TPR by monitoring the signal of H_2O formation (m/e = 18). Because the consumption of CO_2 and H_2 was too small, only the H$_2$-TPR profiles expressed on the basis of H_2O formation are shown in Fig. 10. All three catalysts reveal the formation of H_2O, suggesting that both Ni and Cu metals can be oxidized by CO_2 at 873 K. In our previous work [36], O$_2$-TPO suggests that Cu metal is more easily oxidized by O_2 than Ni metal. The easy oxidation of copper and/or presence of Cu$^+$ on Cu-based catalysts in water-gas shift reaction and methanol synthesis have been well documented [57,58]. Thus, it is deduced that Cu metal is more readily oxidized by CO_2 than Ni metal. For the Ni and Ni-Cu catalysts, the peaks at 515, 678, 760, and 935 K may be assigned to oxygen species associated with Ni metal, whereas the sharp peak appeared at 444 K detected over the Ni-Cu and Cu catalysts can be attributed to oxygen species associated with Cu metal. The reduction temperature of the latter is much lower than that of the former, confirming that oxygen species on Cu metal are more reducible than those on Ni metal. This is
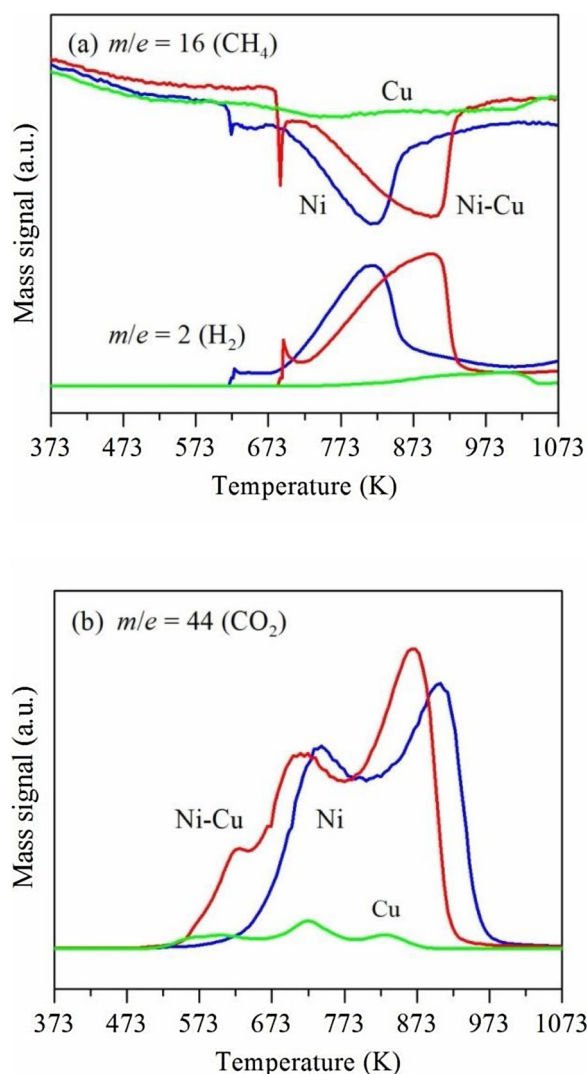
Fig. 9. (a) CH$_4$-TPSR profiles and (b) O$_2$-TPO profiles obtained after CH$_4$-TPSR: (Blue) Ni/Mg(Al)O, (Red) Ni-Cu/Mg(Al)O (Cu/Ni = 0.25), (Green) Cu/Mg(Al)O. (For interpretation of the references to colour in this figure legend, the reader is referred to the web version of this article.)
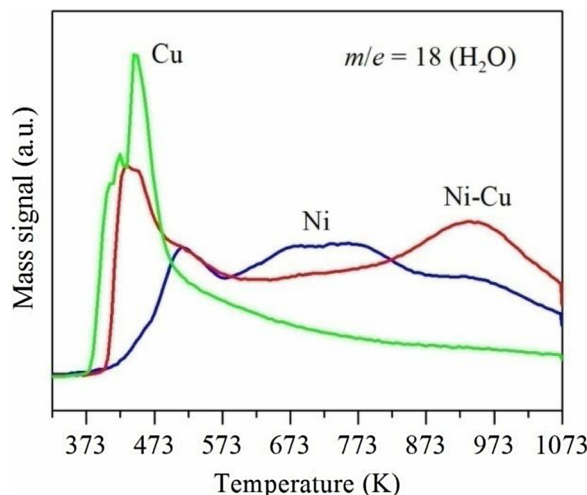
Fig. 10. H$_2$-TPR profiles of catalysts after reduction, followed by CO$_2$-TPSR: (Blue) Ni/Mg(Al)O, (Red) Ni-Cu/Mg(Al)O (Cu/Ni = 0.25), and (Green) Cu/Mg(Al)O. (For interpretation of the references to colour in this figure legend, the reader is referred to the web version of this article.)

in agreement with the fact that copper oxide (CuO or Cu_2O) is higher in reducibility than nickel oxide (NiO) [27,36].

According to proposed mechanism for CH_4-CO_2 reforming [59,60], CH_4 dissociates on the surface of Ni metal to generate CH_x^* ($x = 0-3$) intermediate, and there is dissociative adsorption of CO_2 on the support and/or metal surfaces to yield CO* and O* species; then CH_x^* species react with O* species to produce CO and H_2. When the carbon generation rate is lower than the gasification rate, Ni metal would be oxidized to inactive Ni oxide. In contrast, when the carbon generation rate is higher than the gasification rate, excess carbon may accumulate on the surface to form encapsulating carbon layer, or diffuses through metal particles to form carbon filaments. Therefore, a balance between carbon generation and gasification is critical to achieve stable activity. In this work, coking on Ni/Mg(Al)O is severe in CH_4-CO_2 reforming, and this may be attributed to its high activity for CH_4 dissociation [39]. By alloying Ni with Cu (25%–45%Cu), coke deposition is greatly suppressed. Based on the results of CH_4-TPSR/O_2-TPO and CO_2-TPSR/H_2-TPR studies and those of activation energy measurement, a synergism between nickel and copper that would have a positive effect on coke suppression is suggested. The alloying of Ni with Cu inhibits CH_4 dissociation, causing a reduction in carbon generation rate, while the presence of Cu provides active sites for CO_2 dissociation, promoting the generation of reducible oxygen species for the enhancement of carbon gasification. Overall, a good balance between carbon generation and gasification on the Ni-Cu alloy surface leads to reduced coke deposition and high catalytic stability.

4. Conclusion

The catalytic activity and stability of Ni-Cu/Mg(Al)O catalysts in CH_4-CO_2 reforming are significantly affected by Ni-Cu composition. Under the reaction conditions of $T = 873$ K, $CH_4/CO_2/N_2 = 1/1/2$, SV = 60 000 mL h^{-1} g^{-1}, and TOS = 25 h, the Ni-Cu/Mg(Al)O (Cu/Ni = 0.25–0.5) catalysts show high activity and stability, whereas those with lower and higher Cu/Ni ratios suffer rapid deactivation. Furthermore, the optimized Ni-Cu/Mg(Al)O (Cu/Ni = 0.25) catalyst demonstrates stable activity even at temperature as low as 723 K, functioning well for low-temperature CH_4-CO_2 reforming. The characterization of used catalysts reveals that the nature of coke deposition varies significantly with Ni-Cu composition. A low Cu content (Cu/Ni = 0.1) leads to increased coke deposition, while coke deposition is greatly suppressed at Cu/Ni = 0.25–0.5, with graphitic carbon drastically reduced to about 1/85–1/136 that of Ni/Mg(Al)O, highlighting the positive effect of Ni-Cu alloying on coke suppression. Nonetheless, a higher Cu content (Cu/Ni = 1.0) increases coke deposition due to the formation of Cu-rich alloy. From the catalytic performance and coke deposition, it is concluded that for high catalytic performance, the Ni-Cu composition should be 25–45% Cu. The optimized performance of the Ni-Cu/Mg(Al)O catalyst is related to synergism between nickel and copper. The results of activation energy measurement and CH_4-TPSR/O_2-TPO studies indicate that alloying Ni with Cu inhibits CH_4 dissociation, and the resulting carbon species are more easily gasified. The results of CO_2-TPSR/H_2-TPR suggest that Cu provides active sites for CO_2 dissociation, leading to the formation of active oxygen species. It is suggested that the decrease of CH_4 decomposition and increase of CO_2 dissociation as a result of Ni-Cu alloying are responsible for the suppression of coke deposition.

Acknowledgements

Appendix A. Supplementary data

Supplementary material related to this article can be found, in the online version, at doi:https://doi.org/10.1016/j.apcatb.2018.08.023.

References

[1] M. Fan, A.Z. Abdullah, S. Bhatia, ChemCatChem 1 (2009) 192–208.
[2] C. Liu, J. Ye, J. Jiang, Y. Pan, ChemCatChem 3 (2011) 529–541.
[3] D. Li, Y. Nakagawa, K. Tomishige, Appl. Catal. A Gen. 408 (2011) 1–24.
[4] S. Kawi, Y. Kathiraser, J. Ni, U. Oemar, Z. Li, E.T. Saw, ChemSusChem 8 (2015) 3556–3575.
[5] X. Huang, G. Xue, C. Wang, N. Zhao, N. Sun, W. Wei, Y. Sun, Catal. Sci. Technol. 6 (2016) 449–459.
[6] Z. Bian, I.Y. Suryawinata, S. Kawi, Appl. Catal. B: Environ. 195 (2016) 1–8.
[7] M. Wang, Q. Zhang, T. Zhang, Y. Wang, J. Wang, K. Long, Z. Song, X. Liu, P. Ning, Chem. Eng. J. 313 (2017) 1370–1381.
[8] Q. Chen, J. Zhang, B. Pan, W. Kong, Y. Chen, W. Zhang, Y. Sun, Chem. Eng. J. 320 (2017) 63–73.
[9] Z. Shang, S. Li, L. Li, G. Liu, X. Liang, Appl. Catal. B: Environ. 201 (2017) 302–309.
[10] X. Li, D. Li, H. Tian, L. Zeng, Z.J. Zhao, J. Gong, Appl. Catal. B: Environ. 202 (2017) 683–694.
[11] J.W. Han, J.S. Park, M.S. Choi, H. Lee, Appl. Catal. B: Environ. 203 (2017) 625–632.
[12] P. Djinovic, A. Pintar, Appl. Catal. B: Environ. 206 (2017) 675–682.
[13] B. AlSabban, L. Falivene, S.M. Kozlov, A. Aguilar-Tapia, S. Ould-Chikh, J.L. Hazemann, L. Cavallo, J.M. Basset, K. Takanabe, Appl. Catal. B: Environ. 213 (2017) 177–189.
[14] L. Pino, C. Italiano, A. Vita, M. Lagana, V. Recupero, Appl. Catal. B: Environ. 218 (2017) 779–792.
[15] S. Dama, S.R. Ghodke, R. Bobade, H.R. Gurav, S. Chilukuri, Appl. Catal. B: Environ. 224 (2018) 146–158.
[16] M. Wang, T. Zhao, X. Dong, M. Li, H. Wang, Appl. Catal. B: Environ. 224 (2018) 214–221.
[17] P. Thanh Son, A.R. Sane, B.R. de Vasconcelos, A. Nzihou, P. Sharrock, D. Grouset, M. Doan Pham, Appl. Catal. B: Environ. 224 (2018) 310–321.
[18] X. Zhang, L. Zhang, H. Peng, X. You, C. Peng, X. Xu, W. Liu, X. Fang, Z. Wang, N. Zhang, X. Wang, Appl. Catal. B: Environ. 224 (2018) 488–499.
[19] S. Damyanova, B. Pawelec, R. Palcheva, Y. Karakirova, M.C. Capel Sanchez, G. Tyuliev, E. Gaigneaux, J.L.G. Fierro, Appl. Catal. B: Environ. 225 (2018) 340–353.
[20] S. Das, J. Ashok, Z. Bian, N. Dewangan, M.H. Wai, Y. Du, A. Borgna, K. Hidajat, S. Kawi, Appl. Catal. B: Environ. 230 (2018) 220–236.
[21] D. Halliche, R. Bouarab, O. Cherifi, M.M. Bettahar, Catal. Today 29 (1996) 373–377.
[22] T. Wu, W. Cai, P. Zhang, X. Song, L. Gao, RSC Adv. 3 (2013) 23976–23979.
[23] T. Wu, Q. Zhang, W. Cai, P. Zhang, X. Song, Z. Sun, L. Gao, Appl. Catal. A: Gen. 503 (2015) 94–102.
[24] J. Zhang, H. Wang, A.K. Dalai, J. Catal. 249 (2007) 300–310.
[25] N. Rahemi, M. Haghighi, A.A. Babaluo, S. Allahyari, M.F. Jafari, Energy Convers. Manage. 84 (2014) 50–59.
[26] X. Yu, F. Zhang, W. Chu, RSC Adv. 6 (2016) 70537–70546.
[27] J.H. Lee, E.G. Lee, O.S. Joo, K.D. Jung, Appl. Catal. A: Gen. 269 (2004) 1–6.
[28] H.W. Chen, C.Y. Wang, C.H. Yu, L.T. Tseng, P.H. Liao, Catal. Today 97 (2004) 173–180.
[29] M. Sharifi, M. Haghighi, F. Rahmani, S. Karimipour, J. Nat, Gas Sci. Eng. 21 (2014) 993–1004.
[30] Y.M. Dai, C.Y. Lu, C.J. Chang, RSC Adv. 6 (2016) 73887–73896.
[31] S. Haag, M. Burgard, B. Ernst, J. Catal. 252 (2007) 190–204.
[32] F.A. Silva, C.E. Hori, S.A.M. da, L.V. Mattos, J. Munera, L. Cornaglia, F.B. Noronha, E. Lombardo, Catal. Today 193 (2012) 64–73.
[33] D.S.A. Simakov, M.M. Wright, S. Ahmed, E.M.A. Mokheimer, Y. Roman-Leshkov, Catal. Sci. Technol. 5 (2015) 1991–2016.
[34] M. Koike, D. Li, Y. Nakagawa, K. Tomishige, ChemSusChem 5 (2012) 2312–2314.
[35] D. Li, M. Koike, L. Wang, Y. Nakagawa, Y. Xu, K. Tomishige, ChemSusChem 7 (2014) 510–522.
[36] D. Li, M. Koike, J. Chen, Y. Nakagawa, K. Tomishige, Int. J. Hydrogen Energy 39 (2014) 10959–10970.
[37] D. Li, M. Lu, K. Aragaki, M. Koike, Y. Nakagawa, K. Tomishige, Appl. Catal. B: Environ. 192 (2016) 171–181.
[38] F. Cavani, F. Trifirò, A. Vaccari, Catal. Today 11 (1991) 173–301.
[39] D. Li, S. Xu, K. Song, C. Chen, Y. Zhan, L. Jiang, Appl. Catal. A: Gen. 552 (2018) 21–29.
[40] R. Debek, M. Radlik, M. Motak, M.E. Galvez, W. Turek, P. Da Costa, T. Grzybek, Catal. Today 257 (2015) 59–65.
[41] R. Dębek, M. Motak, M.E. Galvez, T. Grzybek, P. Da Costa, Appl. Catal. B: Environ. 223 (2017) 36–46.
[42] H. Liu, D. Wierzbicki, R. Debek, M. Motak, T. Grzybek, P. Da Costa, M.E. Galvez, Fuel 182 (2016) 8–16.
[43] C. Álvarez Galván, J. Schumann, M. Behrens, J.L.G. Fierro, R. Schlögl, E. Frei, Appl. Catal. B: Environ. 195 (2016) 104–111.
[44] S. Natesakhawat, R.B. Watson, X. Wang, U.S. Ozkan, J. Catal. 234 (2005) 496–508.
[45] S. Sokolov, E.V. Kondratenko, M.M. Pohl, A. Barkschat, U. Rodemerck, Appl. Catal. B: Environ. 113-114 (2012) 19–30.
[46] X. Xie, T. Otremba, P. Littlewood, R. Schomaecker, A. Thomas, ACS Catal. 3 (2013)

224–229.

[47] E.T. Saw, U. Oemar, X.R. Tan, Y. Du, A. Borgna, K. Hidajat, S. Kawi, J. Catal. 314 (2014) 32–46.

[48] C.A. Bernardo, I. Alstrup, J.R. Rostrup-Nielsen, J. Catal. 96 (1985) 517–534.

[49] J.H. Sinfelt, J.L. Carter, D.J.C. Yates, J. Catal. 24 (1972) 283–296.

[50] T.S. Cale, J.T. Richardson, J. Catal. 79 (1983) 378–389.

[51] L.Q. Yang, A.E. Depristo, J. Catal. 148 (1994) 575–586.

[52] I. Alstrup, M.T. Tavares, J. Catal. 139 (1993) 513–524.

[53] A.M. Molenbroek, J.K. Nørskov, B.S. Clausen, J. Phys. Chem. B 105 (2001) 5450–5458.

[54] A.R. Naghash, T.H. Etsell, S. Xu, Chem. Mater. 18 (2006) 2480–2488.

[55] M.C.J. Bradford, M.A. Vannice, Catal. Rev. 41 (1999) 1–42.

[56] T.P.B. Jr, D.W. Goodman, B.D. Kay, J.T.Y. Jr, J. Chem. Phys. 87 (1987) 2305–2315.

[57] I. Atake, K. Nishida, D. Li, T. Shishido, Y. Oumi, T. Sano, K. Takehira, J. Mol. Catal. A: Chem. 275 (2007) 130–138.

[58] T. Shishido, M. Yamamoto, D. Li, Y. Tian, H. Morioka, M. Honda, T. Sano, K. Takehira, Appl. Catal. A: Gen. 303 (2006) 62–71.

[59] L. Foppa, M.C. Silaghi, K. Larmier, A. Comas-Vives, J. Catal. 343 (2016) 196–207.

[60] S.M. Kim, P.M. Abdala, T. Margossian, D. Hosseini, L. Foppa, A. Armutlulu, W. van Beek, A. Comas-Vives, C. Copéret, C. Müller, J. Am. Chem. Soc. 139 (2017) 1937–1949.